Pacific Northwest
NATIONAL LABORATORY

PNNL-35195

Impact of Radiolysis on Iodine Speciation in a Variety of Matrices

September 2023

Brandy N. Gartman
Shirmir D. Branch
Sandra H. Pratt
Andrew M. Ritzmann
Anjelica Bautista
Jason M. Rakos
Caleb Allen
Mark K. Murphy
Maddison A. Heine
Kurt L. Silvers
Nicolas Uhnak

U.S. DEPARTMENT OF ENERGY

Prepared for the U.S. Department of Energy
under Contract DE-AC05-76RL01830

DISCLAIMER

PACIFIC NORTHWEST NATIONAL LABORATORY
operated by
BATTELLE
for the
UNITED STATES DEPARTMENT OF ENERGY
under Contract DE-AC05-76RL01830

Printed in the United States of America

Available to DOE and DOE contractors from
the Office of Scientific and Technical Information,
P.O. Box 62, Oak Ridge, TN 37831-0062
www.osti.gov
ph: (865) 576-8401
fox: (865) 576-5728
email: reports@osti.gov

Available to the public from the National Technical Information Service
5301 Shawnee Rd., Alexandria, VA 22312
ph: (800) 553-NTIS (6847)
or (703) 605-6000
email: info@ntis.gov
Online ordering: http://www.ntis.gov

Impact of Radiolysis on Iodine Speciation in a Variety of Matrices

September 2023

Brandy N. Gartman
Shirmir D. Branch
Sandra H. Pratt
Andrew M. Ritzmann
Anjelica Bautista
Jason M. Rakos
Caleb Allen
Mark K. Murphy
Maddison A. Heine
Kurt L. Silvers
Nicolas Uhnak

Prepared for
the U.S. Department of Energy
under Contract DE-AC05-76RL01830

Pacific Northwest National Laboratory
Richland, Washington 99354

Acknowledgements

The authors wish to thank Samuel A. Bryan for his contributions to help us acquire Raman data. This work was funded under the National Nuclear Security Administration's (NNSA) Office of Conversion (NA-231). PNNL is a multiprogram national laboratory operated for DOE by Battelle Memorial Institute operating under Contract No. DE AC05- 76RL0-1830.

Summary

This report details the work conducted in fiscal year 2023 with the aim of providing a better understanding of the speciation of iodine in support of domestic ^{99}Mo production Shine who uses a sulfate matrix in their process. Laboratory experiments to study the behavior of iodine speciation were conducted using spectroscopic methods including UV-vis and Raman as well as electrochemical studies. Radiolysis occurring in solution presents a unique challenge that is largely unaddressed with thermodynamic modeling, therefore a kinetic model was developed to address these issues. The focus of the studies conducted this year used surrogate radiolytic conditions induced by hydrogen peroxide for comparison to radiolytic conditions from direct gamma irradiation and neat acid solutions. For each case a model incorporating the kinetics was used to predict iodine speciation in the defined conditions where the output was directly compared to the experimental conditions. Further modeling was conducted incorporating the process conditions that are specific to Shine with incorporation of radiolysis and gas sparging.

Acronyms and Abbreviations

PNNL	Pacific Northwest National Laboratory
NNSA	National Nuclear Security Administration
^{99}Mo	Molybdenum 99
HEU	Highly enriched uranium
FY	Fiscal Year
H_2O_2	Hydrogen Peroxide
^{60}Co	Cobalt 60
HNO_3	Nitric Acid
DI water	Deionized water
H_2SO_4	Sulfuric Acid
CV	Cyclic voltammetry, voltammogram
HEF	High Exposure Facility
ORP	Oxidation reduction potential
I^-	Iodine
IO_3^-	Iodate
I_2	Iodine
I_3^-	Triiodide
LOD	limit of detection

Contents

Figures

Tables

1.0 Introduction

The Pacific Northwest National Laboratory (PNNL), as part of the National Nuclear Security Administration's (NNSA) cooperative agreement partnership program, is working in close collaboration on efforts to control the fission gas emissions from domestic ^{99}Mo producers as they stand up their production operations. The ultimate purpose of this program is to develop and support a stable domestic supply of ^{99}Mo that produced without the use of highly enriched uranium (HEU). PNNL has been exploring the fundamental iodine chemistry under the extreme conditions of a solution under high radiolytic stress, while developing a kinetic model that takes the effects of this stress into account to predict iodine speciation. The focus of this effort was to study molecular iodine behavior exposed to either hydrogen peroxide (H_2O_2), as surrogate for radiolysis, or a ^{60}Co gamma source, where both systems are used to alter the solution conditions to mimic conditions of ^{99}Mo fission target solution. Experiments conducted in this report used the hypothesis that hydrogen peroxide would serve as a surrogate for gamma induced radiolysis like that from the ^{60}Co source, a direct comparison of these two systems was also conducted. Similar matrix conditions to the work demonstrated by Graham et. al., were selected to include both oxidizing conditions (i.e., nitric acid) and near neutral conditions (DI water), where the work in FY23 was expanded the focus to including sulfuric acid (H_2SO_4) and sulfates. In addition to continued radiolysis work, experiments were conducted using electrochemistry to probe the reaction mechanisms and gather kinetic data using cyclic voltammetry (CV) to interrogate electrochemical reaction rates. The HNO_3 and H_2SO_4 systems were studied for comparison of iodine behavior. Data collected from the laboratory analysis were intended to provide information which can be incorporated into previously developed thermodynamic equilibrium models and to develop a kinetic model. Ultimately, the goal of these experiments will be to simulate expected conditions based on domestic suppliers, while having a deeper understanding of how the solution redox conditions can impact iodine speciation in the context of fission based ^{99}Mo production, allowing for direct prediction of iodine speciation to aid in direct control of radioiodine.

1.1 Laboratory Experimental Overview

Spectroscopy Characterization Experiments

Initial experiments conducted in FY23 focused on using hydrogen peroxide to induce or simulate radiolysis of the iodine solutions. This was done to mimic radiolysis conditions without the use of the high exposure facility (HEF) at PNNL. Unlike the previous FY, measurements focused on using UV-vis spectrometry, pH and oxidation-reduction potential (ORP) to monitor changes to the solution conditions, since the primary iodine species of interest were iodide (I^-), iodine or molecular iodine (I_2), and triiodide (I_3^-). Of note, the UV-vis spectrometer operated for experiments this year is different than the one used in FY22; therefore, it was important to baseline the instrument against conditions previously analyzed. Experiments were primarily conducted in DI water, dilute HNO_3 (0.5 M), and dilute H_2SO_4 (0.5 M), simulating relevant matrix conditions. Additionally, monitoring changes of the redox conditions was preformed to provide additional data points for to understand. This method was also used to collect kinetic data for the modeling effort, using a feature which continuously collects data. To ensure the results collected from the peroxide studies would be comparable to the previously collected data from the irradiation work with the ^{60}Co source, a second series of dosing studies was conducted. These experiments used the open beam collimated irradiator with a 6780 Ci ^{60}Co source at the HEF. A depiction of the general process using the HEF facility or other "surrogate radiolysis source (i.e., H_2O_2) is shown in Figure 1.

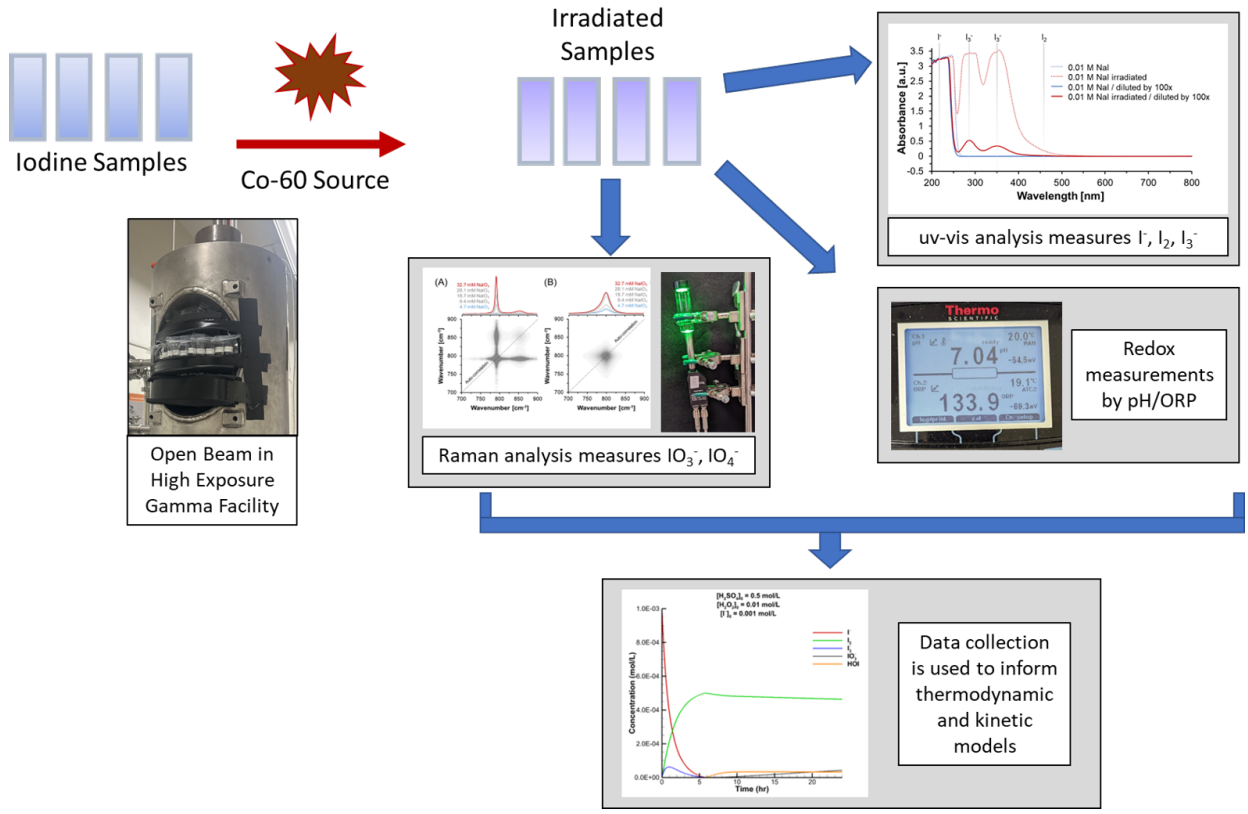

Figure 1. Schematic showing the general process for conducting irradiation experiments. Shown here is the ^{60}Co source which can also represent how the hydrogen peroxide can be used to simulate or induce radiolysis.

Electrochemistry Experiments

Electrochemical experiments were performed where the focus of these studies was to interrogate I^- solutions in either a HNO_3 or H_2SO_4 using a potentiostat to perform peak analysis on the cyclic voltammetry waves. Data collected form these experiments were compared to the spectroscopy studies to understand the iodine speciation and redox couples.

1.2 Modeling Overview

Chemical models were applied to several of the experiments to provide further insight about mechanisms by which the speciation of iodine changes. Two types of models have been developed and described in past reports. Thermodynamic models describe the equilibrium speciation of a solution based on the pH and redox potential of the solution. Kinetic models aim to describe the temporal evolution of the iodine speciation. In principle, the kinetic models should converge to same speciation as the thermodynamic models provided the system is closed. However, there are scenarios where an external influence is applied, and a thermodynamic model simply cannot account for the speciation.

2.0 Methods & Materials

A synergistic effort between experimental and modeling efforts was continued in FY23 using data collected primarily by UV-vis, pH, ORP, and electrochemistry in various matrices for the purpose to improve the kinetic and thermodynamic models currently in development.

2.1 Laboratory Studies

Baseline experiments using DI water and HNO_3 were initially conducted to compare the two UV-vis instruments for work conducted in FY22 and FY23. Upon determining the detection limits and linear range of the new instrument, a variety of testing conditions were examined to study iodine behavior in 1) HNO_3, 2) DI water, and 3) H_2SO_4 and/or sulfate mixtures using H_2O_2 as a source of free radical production. Analysis by UV-Vis used a several different instruments including a Thermo Evolution 220 spectrometer, and an Ocean Optics Flame spectrometer, Ocean Optics DH-Mini light source, and Ocean Optics P-300 fibers. All UV-vis spectra collected used 1 cm pathlength cuvettes with a threaded cap, in all examinations the headspace was minimized to force equilibrium to maximize the concentration of dissolved I_2. This minimizes the effects from gaseous I_2 from leaving solution. These conditions were probed in order to determine oxidation state of aqueous iodine species both as a pure (i.e. un-irradiated) system and to observe changes that occur under radiolysis conditions. Data collected from these experiments included looking at a variety of parameters such as changes to the NaI concentrations, H_2O_2 concentration, acidic matrix, and time. In addition to the various in-situ experiments, a variety of samples were irradiated with the ^{60}Co source for 24 hours, with a resulting dose of 4.752 Mrads. Various matrix conditions were selected, as shown in Table 1, resulting in irradiation solution conditions that mirrored the experimental work with the H_2O_2 studies. Details about the various tests conducted in FY23 are broken down by solution matrix, where the specifics about the various studies for each matrix type is presented in section 3.0.

Table 1. List of matrix conditions analyzed for the open beam dose study.

Matrix Condition	Solution Matrix
1	0.5 M H_2SO_4 -100 µM NaI
2	0.05 M H_2SO_4 -100 µM NaI-0.7 M Na_2SO_4
3	0.05 M H_2SO_4-0.7 M Na_2SO_4
4	0.5 M HNO_3-100 µM NaI
5	0.5 M HNO_3
6	0.5 M HNO_3-100 µM $NaIO_3$
7	DI H_20-100 µM $NaIO_3$

Electrochemical experiments were performed with a BioLogic SP-50 potentiostat. EC-Lab V11.50 software was used to control the potentiostat and perform peak analysis on the cyclic voltammetry waves. The electrodes and electrochemical cell were from Bioanalytical Systems. The working electrode was glassy carbon, the counter electrode was a Pt wire electrode, and the reference electrode was Ag/AgCl. Sulfuric and nitric acid solutions were made from Optima grade concentrated acids from Fisher Scientific. Solutions were bubbled with house nitrogen to remove oxygen. Details of individual experiments are described in Section 5.0.

2.2 Development of the Kinetic Models

Kinetic models have been implemented using established theories and mechanisms taken from the literature.

2.2.1 Kinetic Model

Modeling iodine speciation in ^{99}Mo production requires a kinetic model for several reasons. Open systems present a scenario where the solution may gain or lose certain molecules. Exposure to radiation presents a further complication because the radiation field may exist for a period, and it may change in strength over time. Finally, a kinetic model may be necessary because the time scale for achieving thermodynamic equilibrium exceeds the time in which the solution is observed.

Kinetic models break the chemistry down into the elementary reactions that involve one or two molecules. Likewise, transformations involving numerous electrons in a single step occur in stepwise fashion. The rate, for an elementary reaction ((1) is given according to Equation 2.

$$I^- + I_2 \rightarrow I_3^- \quad (1)$$

$$rate = k_f[I^-][I_2] - k_r[I_3^-] \quad (2)$$

In many cases, breaking down the mechanism into elementary steps necessitates incorporating short-lived species such as radicals. This leads to models that contain a large number of species and a large number of ordinary differential equations to describe how their concentrations evolve.

To model the iodine speciation using chemical kinetics, we employed a detailed mechanism called the LIRIC 3.2 model [Wren and Ball, 2011]. This model contains radiolytic and hydrolytic production of radicals from aqueous matrix, reactions of iodine in oxidation states -1, 0, 1, 3, and 5 with these radicals, and reactions of nitrogen-containing species (e.g., nitrate) with the radicals and iodine-containing species. For further investigation, the interaction of sulfate and sulfuric acid with radicals is also included [Ma, Schmidhammer and Mostafavi, 2014; Jiang et al. 1992; Wojnárovits and Takács, 2019; Criquet and Leitner, 2011]. Finally, mass transfer is incorporated according to the two-film resistance model employed in the LIRIC 3.2 model. The resulting model is solved by formulating the reaction rates and differential equations in python and integrating over time using the initial value problem solver in the scipy package [Virtanen et al., 2020].

3.0 Results & Discussion

Conditions studied this year focused on various matrices relevant to potential domestic ^{99}Mo suppliers. Acidic solutions such as HNO_3 were compared to H_2SO_4 and sulfate matrices or near neutral conditions (DI water) to study the impact the solution matrix has on iodine speciation due to changes in redox states or stress induced by radiolysis. To continue the radiolysis studies this year, surrogate methods to produce radicals needed to be considered simply due to the sample capacity limitations at the HEF facility in either the gamma bunker or open beam collimator. After considering the limited solutions that could be studied with the ^{60}Co, a surrogate method was explored which using H_2O_2 to produce hydroxyl radical (·OH) a primary radiolysis product from water. Hydroxyl radical production is more favored under high gamma and beta dose, like that expected from the dissolved targets for many of the producers. Table 2 contains a larger list of radiolysis products with information on the G-value and reduction potential.

In aqueous solutions, radiolysis products are dependent on the identity and concentrations of matrix constituents. As the concentration of a given constituent increases the likelihood of interaction with a gamma or a spur reaction from a radiolysis event will increase. However, in an aqueous solution the radiolysis will primarily occur with water itself, particularly in solutions of low concentration. As water radiolysis occurs a variety of products are produced with a range of lifetimes. Shorter-lived products are outside the focus of this work; therefore, the focus will only be on those that exist after 10^{-7} s after the

radiolytic event. Production of a given radiolysis product is discussed in terms of the number of molecules produced for a given amount of energy, this value is called a G-value, reported as µmol/J or molecules/100 eV of absorbed energy. A radiolysis product table for water is included below in Table 2.

In addition to considering G-values, rate constants for a given product and the reduction potential for that product are important, dictating the oxidative or reductive power of a given radiolysis product. The reduction potentials for the major radiolysis products are also included in Table 2, as this is the primary means by which these radiolysis products will interact with other constituents in solution.

Therefore, to determine how much H_2O_2 would be needed for each test, calculations using the G-value (0.28 µmol/J) and a dose of 70.9 Mrad were completed. This dose rate was selected based the previous work in [Graham 2023]. Where the calculated value was determined to have a concentration around 0.02 M ·OH produced in the previous irradiation tests and is equivalent to 0.01 M H_2O_2 solution. The equation used for this calculation can be found Appendix A [Pastina and LaVerne 2001, Graham et. al. 2023] Therefore the bulk of the work conducted using the surrogate radiolysis method used a concentration of 0.01 M H_2O_2 as the source of free radicals.

Table 2. Table of select radiolysis product G-Values in µmol/J from water. G-values in parentheses are reported in molecules/100 eV.

Product	G-value (pH 3-11)[a]	G-value (pH 0.5)[a]	Reduction potential (vs NHE)
e^-_{aq}	0.280 (2.70)	0 (0)	-2.9 V[a]
·OH	0.280 (2.70)	0.300 (2.90)	2.7 V[a]
·H	0.060 (0.58)	0.380 (3.65)	-2.3 V[a]
H_2	0.047 (0.45)	0.041 (0.40)	0 V
H_2O_2	0.073(0.70)	0.0081 (0.078)	1.35 V[b]
HO_2·	0.0027 (0.026)	0.00080 (0.0077)	1.05 V[b]
H^+	0.321 (3.10)	-	

[a] Values obtained from Caer 2011
[b] Values obtained from Koppenol, Stanburry, and Bounds 2010
[c] Values obtained from Pastina & LaVerne (2001)

3.1 Iodine in DI water

Due to a transition on the project, the original UV-vis spectrometer was not accessible for use as the primary instrument. Therefore, alternative instruments were used. The baseline experiments used NaI in DI water, where Figure 2 details differences in the data collection between the instruments. Data from both spectrometers showed similar nonlinear trends at higher concentrations. It was also determined that the spectrometer used for the work conducted in FY23 has a concentration limit of 0.2 µM NaI due to nonlinear instrumental response suggesting limited sensitivity at lower iodine concentrations (Figure 3). Above ~0.2 µM NaI, the instrument response became linear indicating the lower limit for the detection of NaI for the Thermo instrument used in FY23. Based on these findings, for the ^{60}Co dose studies that were conducted this FY a concentration of 100 µM NaI was selected for further examination, as a concentration that is within the middle of the linear instrumental range, while being a convenient concentration to make.

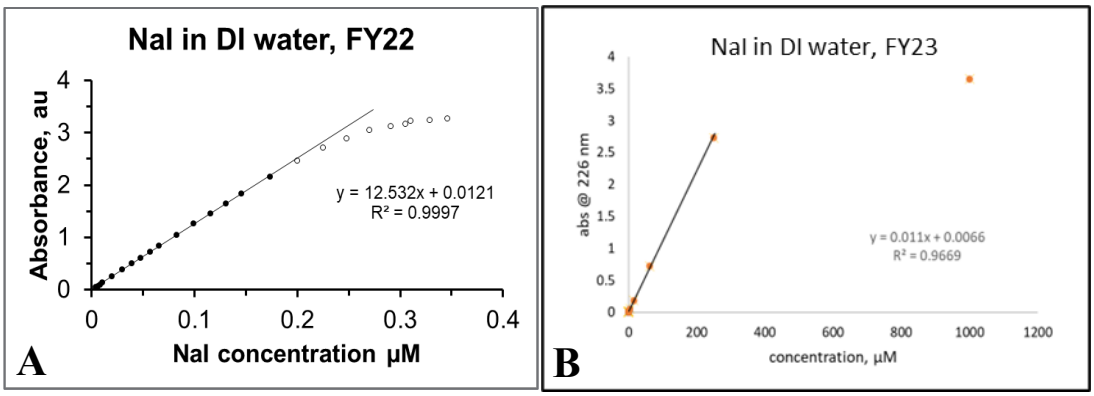

Figure 2. Comparison of the two UV-vis spectrometers used in support of the radiolysis studies.

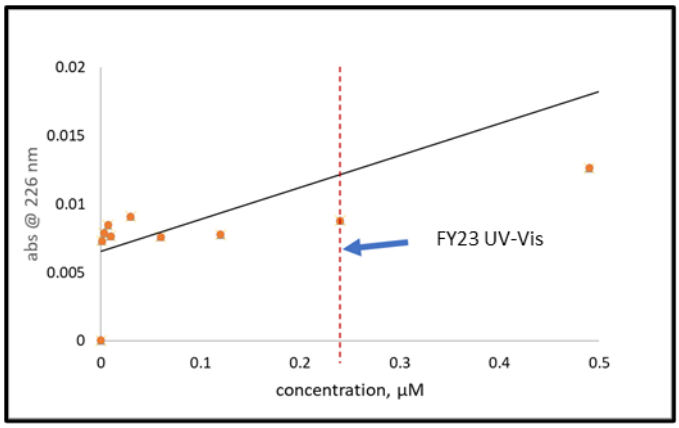

Figure 3. Verification of the limit for stability for the spectrometer used in FY23.

Spectra were collected over a range of NaI concentrations, 0 to 1000 µM, in DI water (Figure 4). In Figure 4A, the peak around 200 nm is the charge transfer peak, while the peak measured at ~226 nm is associated with I^- in solution. The charge transfer peak is the result of electronic excitation of hydrated I^-, between the I and the waters complexing it. In this system, no oxidizer or radical source was present therefore no measurable changes to the speciation were observed across all the concentrations. Figure 4B, shows the relevant absorbance trend across the concentration range that was measured, again this trend shows that at higher concentrations the absorbance signal becomes non-linear.

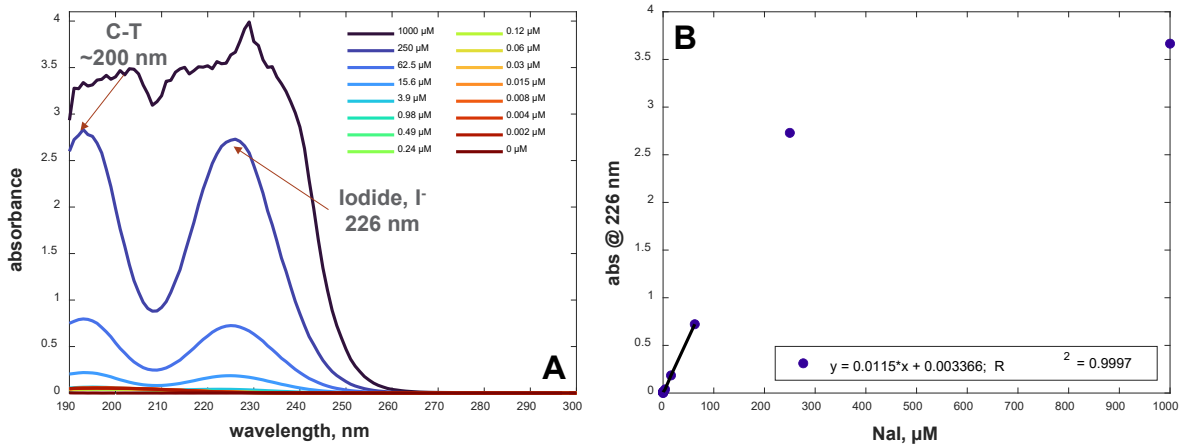

Figure 4. Absorbance of NaI in water (A) UV-vis spectra for NaI at concentrations ranging from 0 – 1000 µM. (B) Absorbance at 226 nm vs. concentration of NaI.

Work reported by Graham et. al. (2023) provided insight about the radiolytic stress on NaI in water. In this work, the presence of I_3^- was detected, and the poorly resolved I_2 and I^- were also observed. To explore the higher oxidation states samples containing 100 µM $NaIO_3$ in DI water were irradiated. The lower oxidation states could be measured using UV-vis, while the IO_3^- species could be measured via Raman analysis. The UV-vis spectra that was collected is shown in Figure 5. While the concentration of $NaIO_3$ was chosen to match the concentrations of NaI used for the UV-Vis experiments, this resulted in spectral signals too low to be measured via Raman, therefore, no Raman data is presented for this test. In the irradiated IO_3^- solution, measurable I^- was found in UV-vis, without a strong indication of I_3^- or I_2, which appear at 290 and 350 nm for I_3^- and 450 nm for I_2. There are no indications of any other absorption from Measurement of the solution conditions, showed the pH decreased for the irradiated solution, becoming acidic, and showed a decrease in the ORP suggesting the solution became reductive (Table 3). Therefore, as radiolysis occurred, the breakdown of water likely caused the production of hydrogen peroxide radicals, which can be an oxidizer or a reducing agent, resulting in the reduction of the $IO_3^-{}_{(aq)}$ to $I^-{}_{(aq)}$ [Pastina and LaVere 2001, Iwamatsu et. al. 2018].

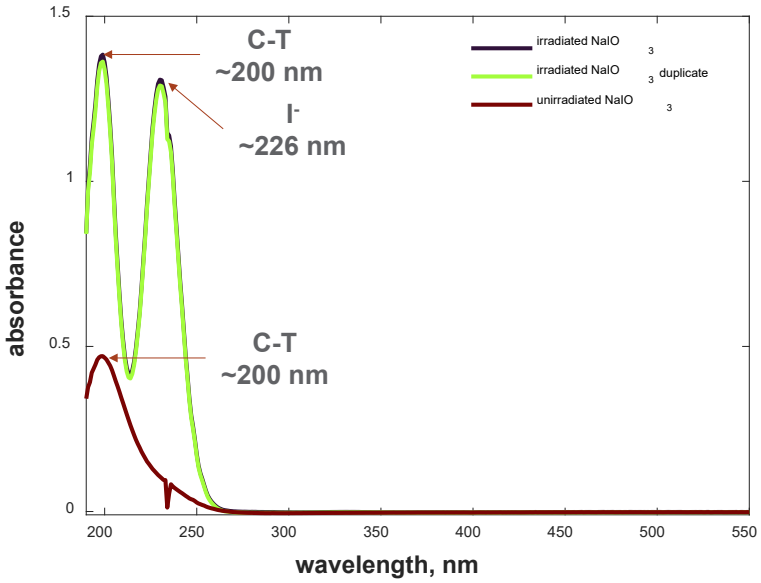

Figure 5. UV-vis spectra of the 100 µM $NaIO_3$ in H_2O for the irradiated and unirradiated solutions.

Table 3. Measured pH and ORP data for the $NaIO_3$ solutions.

Matrix	Irradiation Cond.	pH	ORP
DI H_2O- 100 uM $NaIO_3$	irradiated	4.51 ± 0.55	208.7 ± 8
	unirradiated	6.80 ± 0.34	388.6 ± 6.5

3.2 Iodine in nitric acid

Spectra was collected over a range of NaI concentrations in 0.5 M HNO_3 is shown in Figure 6. In Figure 6A, the rapid formation of I_3^- is observed with no observation of the I_2 species. Where the presence of HNO_3 was shown to have an extremely high absorbance (>4 a.u.) below 300 nm and interferes with the spectral range expected for I^- at ~226 nm. Therefore, any presence of I^- could not be observed due to baseline corrections that were conducted. This phenomenon was also noted in the publication by Graham et. al., 2023. It was reported during preparation of the samples for these measurements the presence of a brown vapor appeared immediately after spiking NaI into the HNO_3. Data was collected after the samples were transferred to the cuvettes, however the brown vapor that formed was likely free I_2 escaping from solution, and therefore not measured in the solutions. An exponential-like response of I_3^- absorbance to [NaI] as shown in Figure 6B was also observed. No pH or ORP data was reported for these experiments. Finally, the spectra collected from the ^{60}Co irradiated solutions in HNO_3 were most likely over corrected from the background solution that was used to baseline the instrument and could not be resolved, so this data will not be reported here.

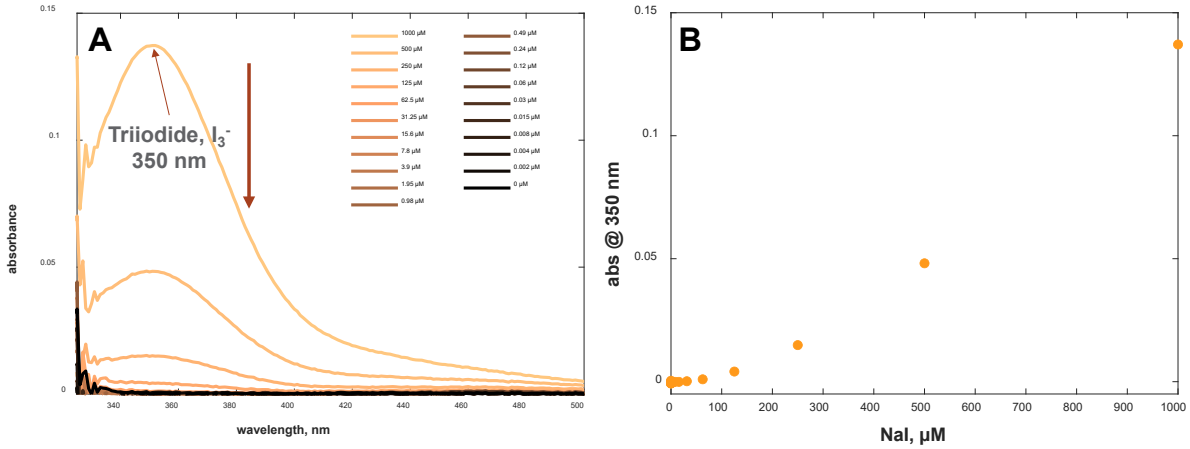

Figure 6. Absorbance of NaI in 0.5 M HNO_3. (A) UV-vis spectra for NaI at concentrations ranging from 0 – 1000 µM. (B) Absorbance at 350 nm vs concentration of NaI.

3.3 Iodine in sulfuric acid

Like the studies conducted in DI water and HNO_3, a range of NaI concentrations were first measured in 0.5M H_2SO_4 in order to baseline the solution matrix without the radiolysis stress or influence of free radicals. Over the range of concentrations analyzed, 0 to 1000 µM, of I^- in solution only the 200 nm charge transfer peak and I^- peak at ~226 nm was measured, indicating no other iodine species was present in solution. The detection response was no longer linear at data points greater than 250 µM and the limit of detection (LOD), shown in Figure 7B. Redox data for these samples also collected and showed no observed trends in the reported pH (~0) values. Whereas the ORP data, shown in Figure 8, measured the redox environment trended towards more reducing conditions as the I^- concentration increased. This leads us to believe the sulfate matrix will be beneficial to the overall solution chemistry, and further interrogation of changes to this matrix caused by radiolysis products will be of value.

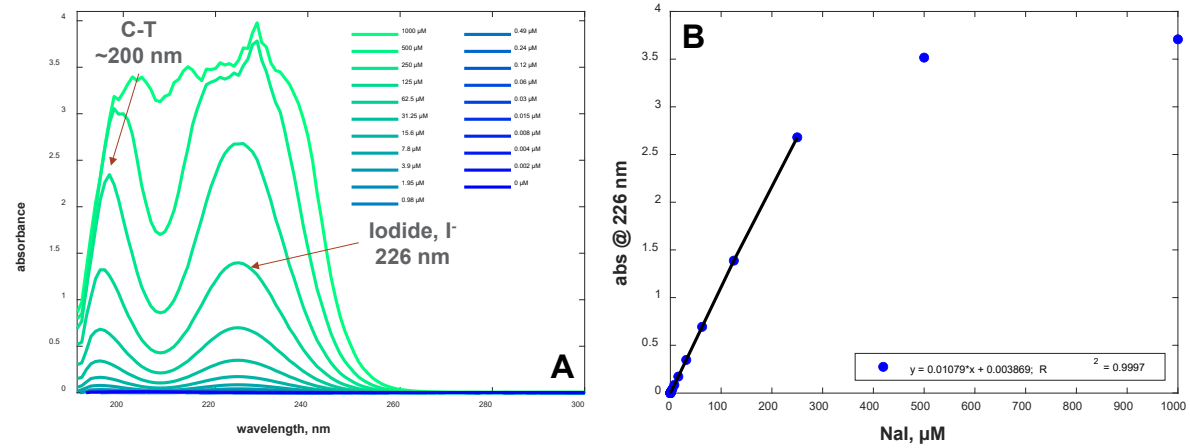

Figure 7. Absorbance of NaI in 0.5 M H_2SO_4. (A) UV-vis spectra for NaI at concentrations ranging from 0 – 1000 µM. (B) Absorbance at 226 nm vs concentration of NaI.

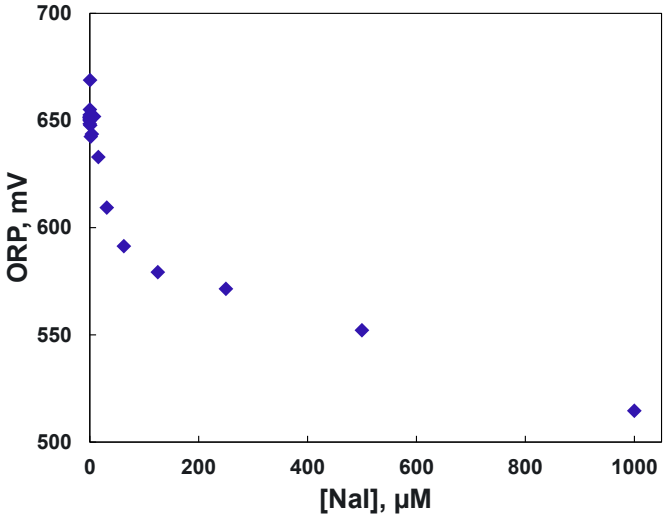

Figure 8. Oxidation-reduction potentials of NaI in 0.5 M H_2SO_4.

Next, studies were conducted by spiking in 0.01 M H_2O_2 to the 0.5 M H_2SO_4 across various concentrations of NaI. Measured changes to the solution chemistry are shown in Figure 9, where all data points shown were measured within 30 mins of solution preparation. Figure 9A shows the UV-vis spectra that was collected after the peroxide was added to this system for wavelengths expected for the . In general, no significant changes to the I- species were observed, however, there appears to be some conversion of the I^- to I_3^- and I_2 as shown in Figure 9B. The I_3^- and I_2 peaks are measurable only initially in the samples with higher concentrations of NaI. In the kinetic studies (section 3.4) a select NaI concentration was measured overtime to provide more data about changes to the speciation. Unfortunately, no pH and ORP data was collected for these solutions due to issues with the probes.

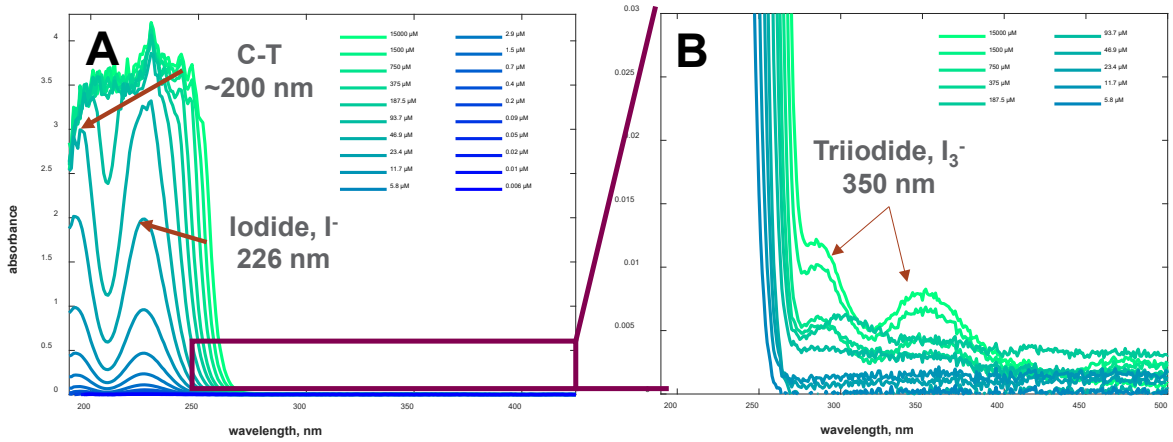

Figure 9. Absorbance of NaI in 0.5 M H_2SO_4 with 0.01 M H_2O_2. (A) UV-vis spectra for NaI at concentrations ranging from 0 – 15000 µM. (B) Inset of UV-vis spectra at select NaI concentrations to show the ingrowth of the I_3^- and I_2 peaks.

For comparison to the hydrogen peroxide studies, samples in either 0.5 M H_2SO_4 or a mixed sulfate matrix, made to be a surrogate for the solution used by a ^{99}Mo producer, were irradiated using the ^{60}Co source. Data from these experiments is found in Figure 10 and Figure 11, with the pH and ORP data in Table 4. Though these solutions have different matrices, the UV-Vis active components are equal in concentration, therefore they are expected to have similar UV-Vis response, however it is expected that the

effects from radiolysis will scale with the increasing concentration of the SO_4^{2-}. As seen in both data sets, either 0.5 M H_2SO_4 or the mixture of 0.05 M H_2SO_4- 0.7 M Na_2SO_4, there was a measurable I_2 peak and a suspected I_3^- peak that was measured on the shoulder of the charge transfer peak and/or potential sulfate interference. When comparing these samples to the unirradiated samples, the evidence of the transformation is clearly observed since the I^- peak at 226 nm is the only measurable peak in the unexposed reference sample.

Redox measurements were also collected for this data set. No significant changes to the pH were observed but this will be used to feed into the kinetic model. Whereas the ORP data shows measurable changes to the redox conditions in the solution matrix between the irradiated and unirradiated samples. In the samples containing 100 µM NaI- 0.5 M H_2SO_4, there was an increase in the solution potential post-irradiation to promotes the I_2 formation. The spectra in Figure 10 support this with good agreement between the replicates. The formation of I_3^- is also supected but the peaks are not clear in the specta.

When comparing to the samples with the mixed sulfate matrix (i.e., 100 µM NaI-0.05 M H_2SO_4- 0.7 M Na_2SO_4 and 0.05 M H_2SO_4- 0.7 M Na_2SO_4) the redox conditions measured in the post-irradiation solution were reducing. This suggests that the addition of the Na_2SO_4 has potentially undergone a decomposition reaction forming Na_2SO_3 (Equation 3), reducing agent, which can reduce the $I_{2\,(aq)}$ back to $I^-_{(aq)}$ [Tenchurina and Sal'keeva 2015, Jiang et. al. 1992].

$$SO_4^{2-} + H^0 \rightarrow SO_3^{2-} + OH^- \tag{3}$$

More detailed studies related to the kinetics of this reaction should be conducted to further probe changes to redox conditions with time. Data shown in Figure 11 shows some variations in the measured replicates, however there is still the presence of molecular iodine. The suspected I_3^- peaks appear to be possibly overlapping with interferences from the sulfate since there are shoulders in this region, to variable degrees, for the both the irradiated mixed sulfate samples and the unirradiated reference samples.

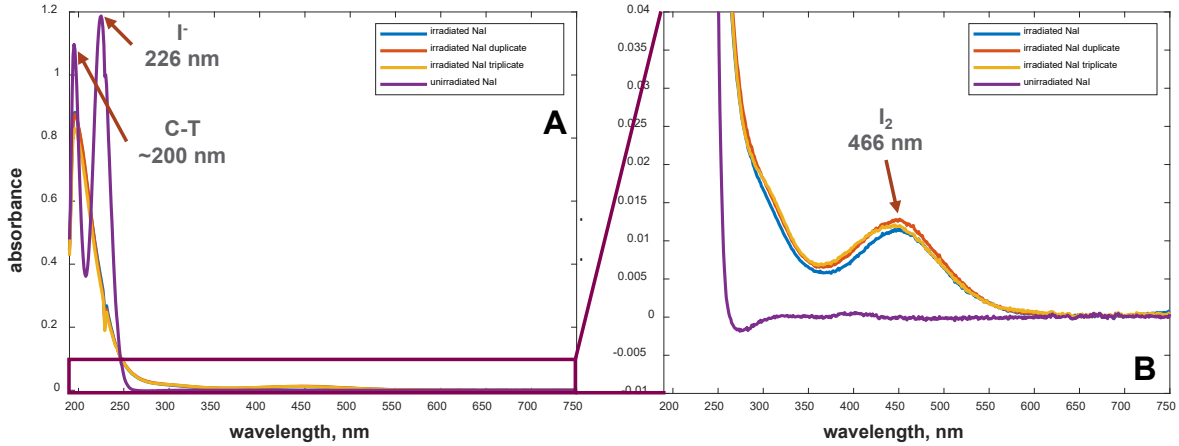

Figure 10. Absorbance of 100 µM NaI in 0.5 M H_2SO_4 radiolysis. (A) UV-vis spectra of irradiated solutions compared to unirradiated solution. (B) Inset of UV-vis spectra of irradiated solutions compared to unirradiated solution.

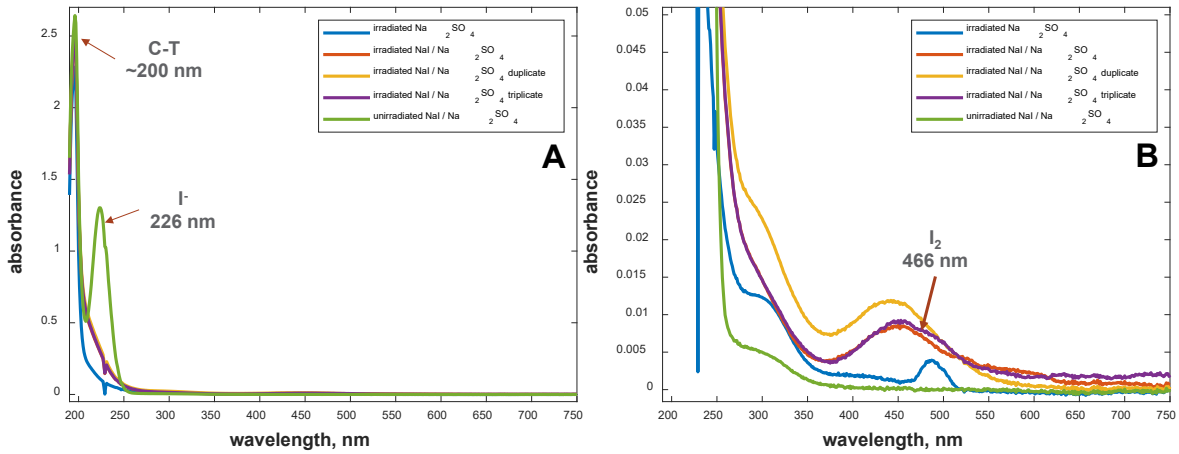

Figure 11. Absorbance of 100 µM NaI and 0.7 M Na_2SO_4 in 0.05 M H_2SO_4 radiolysis. (A) UV-vis spectra of irradiated solutions compared to unirradiated solution. (B) Inset of UV-vis spectra of irradiated solutions compared to unirradiated solution.

Table 4. Measured pH and ORP data from the irradiated samples containing sulfate.

Matrix	Irradiation Cond.	pH	ORP
100 µM NaI - 0.5 M H_2SO_4	irradiated	0.49 ± 0.01	534.5 ± 165.5
	unirradiated	0.52	469.6
100 uM NaI-0.05 M H_2SO_4 - 0.7M Na_2SO_4	irradiated	1.94 ± 0.01	156.0 ± 26.4
	unirradiated	1.93	426.4
0.05 M H_2SO_4 - 0.7M Na_2SO_4	irradiated	1.91	202.7
	unirradiated	1.91	358.3

3.4 Kinetic Study

Time dependence experiments were also conducted to help understand the kinetics associated with the formation of I_2 and I_3^-, where spectra were collected using the UV-vis in a continuous mode over the course of hours. Three different conditions were measured to look at how radiolytic stress influences NaI in HNO_3 and H_2SO_4 over time for comparison to $NaIO_3$ in HNO_3 with time.

Figure 12 depicts the data collected over ~ 2 hours for solution containing 0.2 mM NaI-0.5 M H_2SO_4 with 0.01M H_2O_2 used as an analog to radiolysis of water. In the spectra there is clear ingrowth of I_3^- and I_2 peaks at (~270-280 nm and ~350 nm for I_3^-, and ~460 nm and I_2) along with a consumption of the I^- (~226 nm) during the collection time. This figure depicts the overall reaction mechanisms as outlined in (4)(6). These reaction mechanisms have also been previously outlined by Sawai et. al. 1966 when they were looking at radiolysis effects on KI. Since the data collected in this study is timestamped it will provide more details about the reaction rates for the kinetic model in development. Over time the I^- was oxidized to I_2, which appears to be consumed in the formation of I_3^-. The I_3^- disappeared over time as the I_2 grows in, while still maintaining a significant amount of the starting I^-. Though further analysis is needed examining longer times, it appears that the I_3^- is a temporary species and I_2 becomes the primary species of molecular iodine. This change in speciation is not thought to be the consequences of equilibrium related to loss of gaseous species. This could have implications on processing.

$$2I^- + H_2O_2 \xrightarrow{H^+} 2I + 2H_20 \quad (4)$$

$$I^- + I^- \rightarrow I_2 + 2e^- \quad (5)$$

$$I_2 + I^- \leftrightarrow I_3^- \quad (6)$$

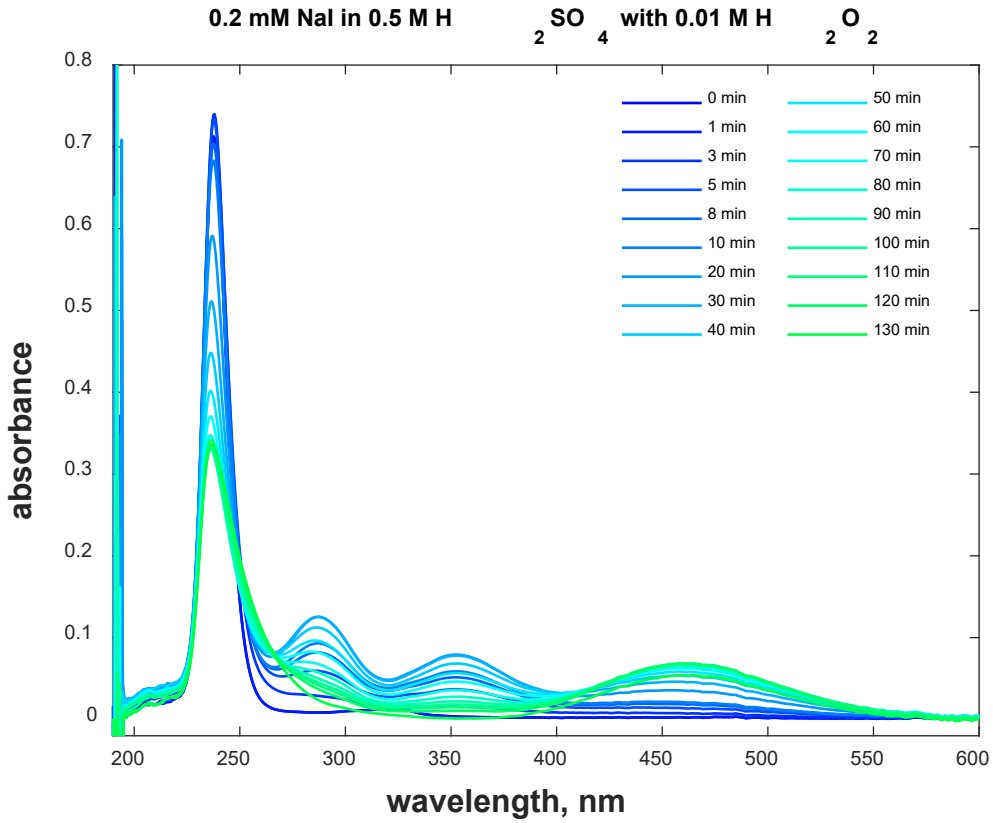

Figure 12. Kinetic study using H_2O_2 to induce radiolysis for measuring speciation changes of the dissolved NaI in 0.5M H_2SO_4 over ~2 hrs. Spectra show in this figure are select data points collected from 0 minutes up to 130 minutes.

4.0 Electrochemistry

The oxidation of iodide to iodine was studied in 0.5 M H_2SO_4, 0.5 M HNO_3 and 3 M HNO_3. A cyclic voltammogram of 1 mM iodide (as potassium iodide) in 0.5 M H_2SO_4 is shown (Figure 13). The redox waves are identified in Equation 7-12 [Yaraliev 1982]:

$$\text{A1: } I^- \rightarrow \frac{1}{2}I_2 + e^- \quad (7)$$

$$\text{and } 2I_3^- \rightarrow 3I_2 + e^- \quad (8)$$

$$\text{A2: } \frac{1}{2}I_2 + 3H_2O \rightarrow IO_3^- + 6H^+ + 5e^- \quad (9)$$

$$\text{C1: } IO_3^- + 6H^+ + 5e^- \rightarrow \frac{1}{2}I_2 + 3H_2O \quad (10)$$

$$\text{C2: } \frac{1}{2}I_{2(ads)} + e^- \rightarrow I^- \quad (11)$$

$$\text{C3: } \frac{1}{2}I_2 + e^- \rightarrow I^- \quad (12)$$

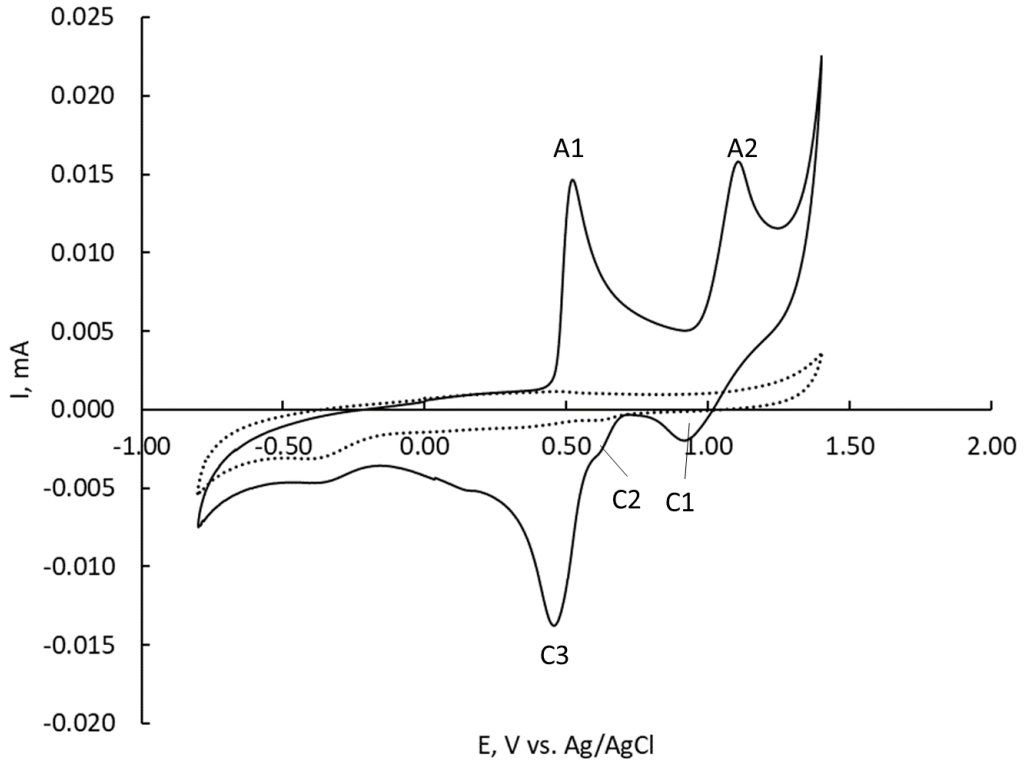

Figure 13. Cyclic voltammogram of 0.5 M H_2SO_4 (dotted line) and 1 mM KI in 0.5 M H_2SO_4 (solid line) at a glassy carbon electrode. Scan rate 20 mV/s.

The electrochemical iodide/iodine redox wave A1/C3 Equation 7 & 12 appears reversible in Figure 13 while the iodine/iodate redox wave A2/C1 Equation 9 & 10 is clearly irreversible, indicated by the stark difference between their peak current and peak shape. The small shoulder C2 is believed to be reduction of iodine that has been adsorbed onto the electrode. Further analysis of the iodide/iodine redox wave indicated that this electrochemical reaction is quasi-reversible. Since iodate formation is unlikely under radiolysis conditions in a sulfuric acid system, the iodide/iodine redox couple was chosen to analyze further at variable scan rates. Results for 0.5 M H_2SO_4 are shown in Table 5.

Table 5. Effect of scan rate on iodide/iodine redox couple in 0.5 M H_2SO_4. [KI] = 1 mM.

Scan Rate, mV/s	*Reduction Peak Position, V vs. Ag/AgCl*	*Reduction Peak Height, mA*	*Oxidation Peak Position, V vs. Ag/AgCl*	*Oxidation Peak Height, mA*	*ΔE_p, mV*	*I_a/I_c*

1	0.461	0.00267	0.518	0.00213	57	0.798
2	0.462	0.00360	0.511	0.00261	49	0.726
5	0.462	0.00518	0.512	0.00491	50	0.948
10	0.459	0.00716	0.511	0.00650	52	0.908
20	0.452	0.0115	0.514	0.0101	63	0.876
50	0.442	0.0190	0.520	0.0170	78	0.895
100	0.432	0.0262	0.528	0.0233	96	0.887

Peak height increases in proportion with the square root of the scan rate per the Randles-Sevcik equation (Equation 13) (Figure 14), indicating that the redox waves are diffusion controlled and not adsorbed [Wang 2000]. However, it is believed that some adsorbed I_2 is also present, as supported by the C2 wave in Figure 13, and may also be the reason for the observed ΔE_p, which should be 59 mV for a one-electron transfer in a purely diffusion-controlled system, and yet, less than 59 mV was observed for the lower scan rates.

$$i_p = (2.69 \times 10^5) n^{3/2} A C D^{1/2} \upsilon^{1/2} \quad (13)$$

In Equation 13, i_p is the peak current in amps, n is the number of electrons transferred (1 for iodide/iodine), A is the area of the electrode (0.0804 cm^2), C is the concentration of the redox couple in mol/mL (the solution was 1.1 x 10^{-6} mol/mL), D is the diffusion coefficient for reactant (1.95 x 10^{-5} cm^2/s for iodide, 1.36 x 10^{-5} cm^2/s for iodine) [Cantrel 1997], and υ is the scan rate in V/s.

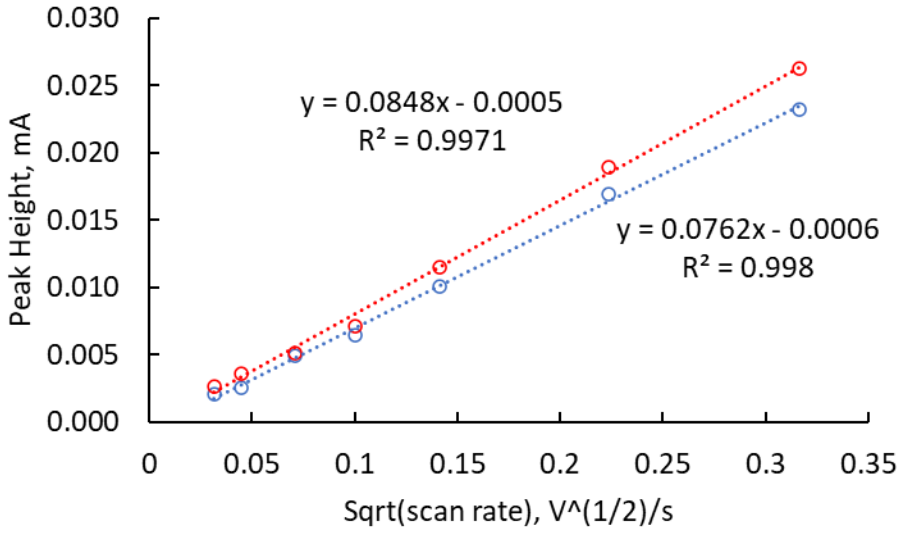

Figure 14. Peak height of cyclic voltammogram waves plotted against the square root of the scan rate. Red trace: reduction wave, blue trace: oxidation wave.

The theoretical peak current for this system calculated using Equation 13 is approximately 1.1 times the observed peak current due to the quasi-reversibility of the redox couple. For a quasi-reversible redox couple, a slightly altered version of the Randles-Sevcik equation can be used (Equation 14) [Wang 2000].

$$i_p = (2.99 \times 10^5) n (\alpha n)^{1/2} A C D^{1/2} \upsilon^{1/2} \quad (14)$$

Since peak current i_p was observed, and all the other values are known, the transfer coefficient, α, may be calculated to provide information about the symmetry of the energy barrier of the reaction [Bard 2001]. If

oxidation and reduction reactions have equal energy barriers, α is 0.5. Using Equation 14, α = 0.76, indicating the redox reaction is asymmetrical. Since α is greater than 0.5 it indicates that reduction of I_2 to I^- has a significantly higher energy barrier than oxidation of I^- to I_2.

Another parameter that can be estimated from these data is the standard rate constant k^0, which is an indication of how rapidly the redox products reach equilibrium, with higher k^0 values indicating more rapid equilibrium. A quasi-reversible system will have a k^0 between 0.1 and 10^{-5} cm/s. Fully reversible systems have $k^0 > 0.1$ and irreversible system have $k^0 < 10^{-5}$ cm/s [Wang 2000]. ΔE_p can be used to estimate k^0 for quasi-reversible redox reactions according to the Nicholson method since ΔE_p becomes greater than 59/n mV at high scan rates for quasi-reversible systems (Equation 15) [Nicholson 1965].

$$\psi = \frac{\gamma^{\alpha} k^0}{\sqrt{\pi a D_O}} \tag{15}$$

Values for ψ, which is a dimensionless rate parameter in cyclic voltammetry, are provided in the reference according to the ΔE_p [Nicholson 1965]. Larger ΔE_p means a smaller ψ, whose range is between 0.1 and 20 before the model is no longer valid: (1.48 was used for the 50 mV/s observation in Table 5). In Equation 15, γ is the square root of (D_O/D_R) which are the diffusion coefficients of iodine and iodide respectively, α is the transfer coefficient calculated above, a is nFυ/RT where n is the number of electrons transferred, F is the faraday constant (96,485 coulombs/mol), υ is the scan rate in V/s, R is the ideal gas constant (8.3145 J/mol•K), and T is the temperature in kelvin (298 K).

The k^0 that was calculated for the iodide/iodine redox couple in 0.5 M H_2SO_4 was 0.015 cm/s putting the electrochemical redox reaction in the quasi-reversible range.

Nitric acid (0.5 M) was also investigated and had a transfer coefficient α of 0.56 and a k^0 of 0.05 cm/s indicating an energy barrier that only slightly favors oxidation of I^- to I_2 compared with the sulfuric acid media and that the reaction in sulfuric acid reaches equilibrium slightly faster than in 0.5 M sulfuric acid. More details about the nitric acid medium (including 3 M HNO_3) are in PNNL-35047.

Iodide was not chemically oxidized in 0.5 M sulfuric acid without an added oxidizer. However, with the addition of hydrogen peroxide, iodide was oxidized to iodine (see Eq (4) and (5)) after approximately 10 minutes. In order to probe the chemical reaction with electrochemical techniques, the solution was stirred so that the diffusion layer of the electrode would be infinite. In this way, the redox species in solution could be analyzed without perturbing the oxidation states of ions at the surface of the electrode with the electrochemical measurements.

The potential range of the iodide/iodine redox couple as determined in Figure 13 was scanned with convection using a magnetic stir bar. Initially, only anodic current was observed because the solution contained only iodide and no I_2. After the first cyclic voltammogram, 0.1 M H_2O_2 was added. The anodic current was diminished by the fourth CV, and cathodic current increased with the formation of I_2. These results are similar to those observed in the UV-vis experiments, although the H_2O_2 concentration was 0.01 M in the UV-vis experiments and 0.1 M in the electrochemical experiments. Gradually, the cathodic current was also decreased with no return of the anodic current indicating that iodine was not being reduced back to iodide (Figure 15). It is believed that I_2 was either volatilizing or becoming inaccessible to the electrode as a solid.

It does not appear from this experiment that a significant amount of triiodide formed in the sulfuric acid matrix, although it did form in the nitric acid matrix [PNNL-35047] and well as being observed in the UV-vis experiments (see Figure 12). Since the oxidation of iodide and triiodide occur at very near the same potential, the anodic current in Figure 15 would not immediately decrease if a significant amount triiodide

formed in first. The discrepancy on triiodide between the UV-vs and electrochemistry experiments may be a matter of method sensitivity: absorbance spectroscopy is more sensitive for these analytes.

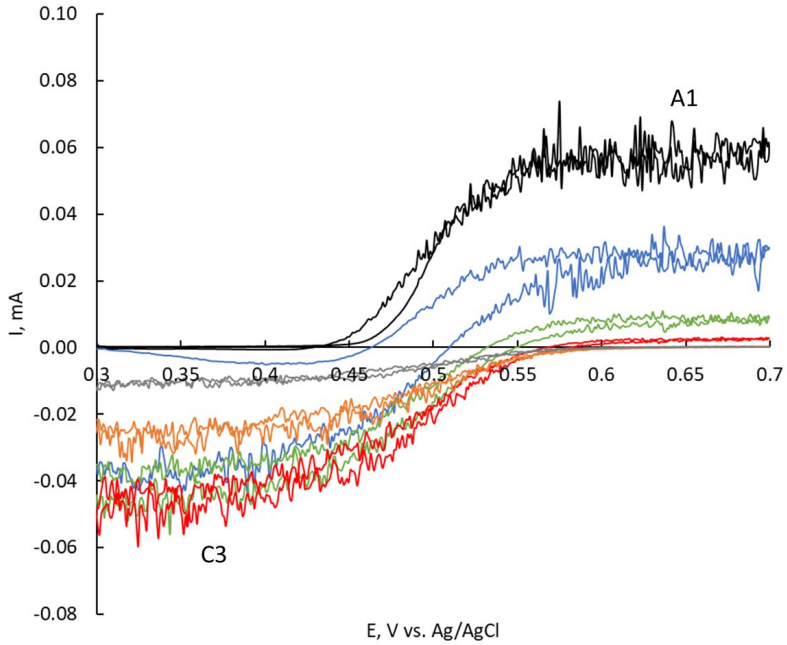

Figure 15. Cyclic voltammogram of 2 mM iodide (as KI) in 0.5 M H_2SO_4 after addition of 0.1 M H_2O_2 with convection at a glassy carbon electrode. Scan rate 5 mV/s. Black trace: before addition of H_2O_2, blue trace: first CV after addition of H_2O_2, green trace: second CV after addition of H_2O_2, red trace: third CV after addition of H_2O_2, orange trace: 25th CV after addition of H_2O_2, gray trace: 50th CV after addition of H_2O_2.

The examination of the effects of the addition of H_2O_2 was performed for three different concentrations of KI. The decreasing anodic current (Figure 16) and the increasing then decreasing cathodic current (Figure 17) were plotted against time. The behavior was independent of the initial iodide concentration, including the time at which the I_2 concentration reached its peak, which is approximately 8 minutes, based on the cathodic current (Figure 17).

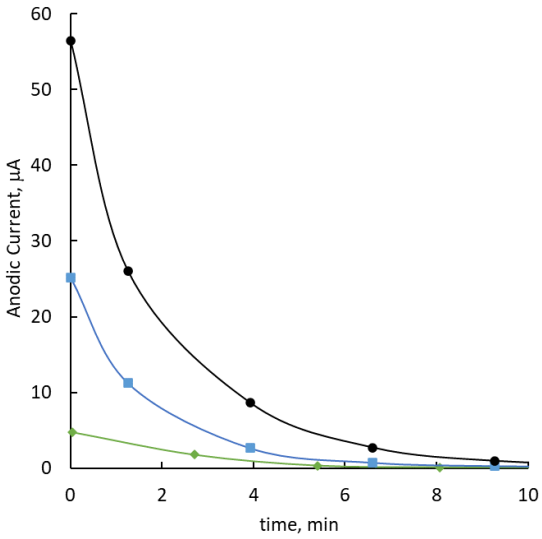

Figure 16. Anodic current in iodide CV over time in 0.5 M H_2SO_4 after addition of 0.1 M H_2O_2 with convection. Black: 2 mM KI, blue: 1 mM KI, green: 0.1 mM KI. Anodic current is proportional to iodide concentration in solution.

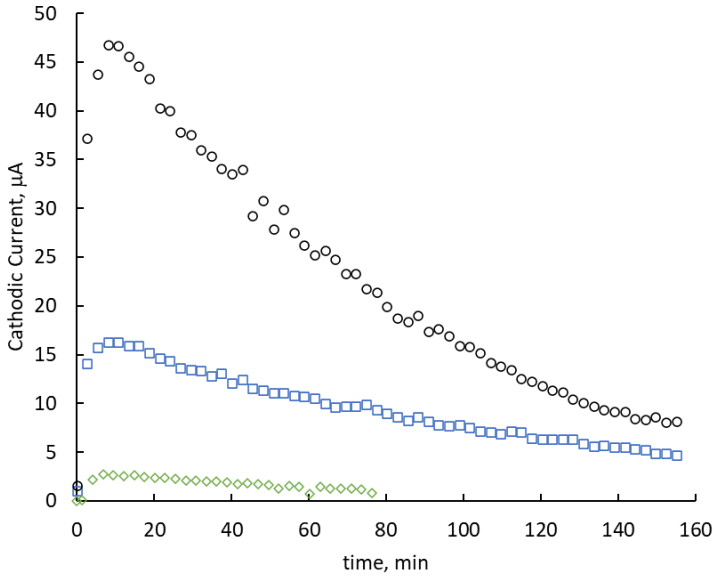

Figure 17. Cathodic current in iodide CV over time in 0.5 M H2SO4 after addition of 0.1 M H2O2 with convection. Black: 2 mM KI, blue: 1 mM KI, green: 0.1 mM KI. Cathodic current is proportional to iodine concentration in solution.

Instead of using cyclic voltammetry, similar data can be collected using chronoamperometry. In these experiments, the potential was held constant such that either oxidation or reduction of the iodide/iodine redox couple would occur (Figure 18). The solution was agitated so that if no reaction were occurring, a steady (though noisy) current would be observed. In a quiescent solution the current decreases due to the diffusion layer being exhausted of reactants. Chronoamperometry is a much simpler method to gather reaction rate data. However, cyclic voltammetry has the advantage of gathering information from both oxidation states and should be done initially. Note also that the chronoamperometry experiments used a higher KI concentration than the CV experiment (5 mM). After the experiment, solid I_2 was visible in the

electrochemical cell (Figure 19), although it was not noticed for any of the other concentrations. This indicates that insolubility of I_2 could be at least partially responsible for the decrease in the cathodic current after the iodide and the anodic current are eliminated.

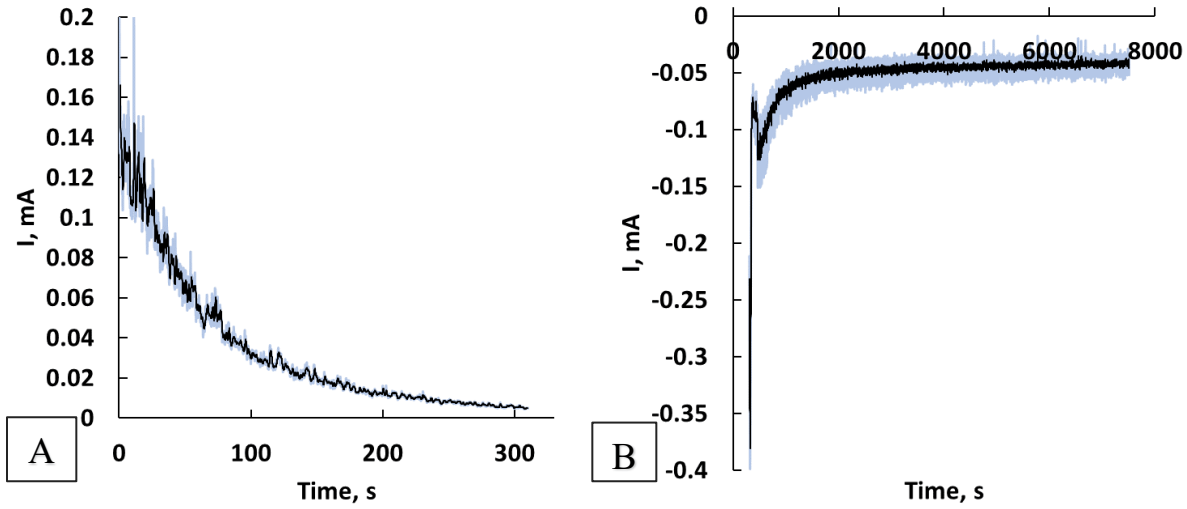

Figure 18. Chronoamperograms for 5 mM iodide (and KI) in 0.5 M H_2SO_4 with addition of 0.1 M H_2O_2 (added 10 s after start of **A**). **A**: Applied potential +0.70 V vs. Ag/AgCl, **B**: Applied potential +0.30 V vs. Ag/AgCl.

Figure 19. Photograph of 5 mM iodide solution in 0.5 M H_2SO_4 after completion of chronoamperometry experiment with addition of 0.1 M H_2O_2.

Volatilization of I_2 is also thought to contribute to the loss of cathodic current but may be a result of convection. The experiment in Figure 15 was repeated in a quiescent solution (Figure 20). In quiescent solution, it takes much longer for the anodic current due to oxidation of iodide to decrease (3 hours instead of 10 minutes). However, the methods should not be compared directly, since iodide could be eliminated in the bulk of solution but still be present at the diffusion layer of the electrode from the oxidation scan. The cathodic current also stars to decrease after approximately 5 hours whereas in an agitated solution the cathodic current is halved after approximately 1 h. Therefore, convection significantly speeds up the volatilization of iodine, but even without convection it does occur. It should also be noted that the electrochemical cell was not gas-tight.

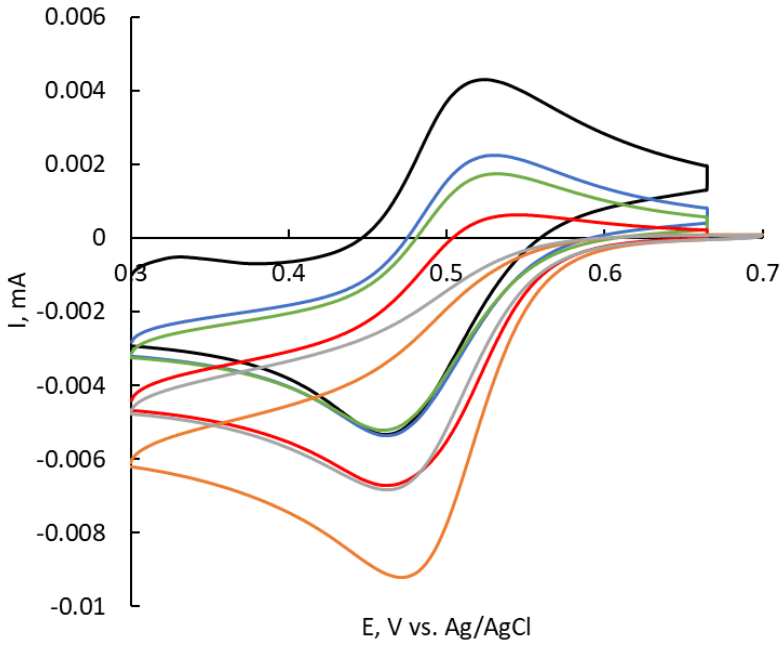

Figure 20. Cyclic voltammogram of 1 mM iodide (as KI) in 0.5 M H_2SO_4 with addition of 0.1 M H_2O_2 in quiescent solution. CV's shown are 5 (black), 8 (blue), 30 (green), 200 (red), 300 (orange) and 375 (gray) minutes after addition of H_2O_2.

Electrochemistry is a powerful tool for speciation analysis. However, more work would be needed to achieve full benefit of these methods. Ideally, several concentrations of sulfuric acid and hydrogen peroxide would be compared to develop a rate law for the reactions. Conditions such as temperature, ionic strength, pH and stirring speed could also be evaluated. Convection experiments should be performed with a rotating cell or rotating disk electrode instead of a magnetic stir bar for consistent results. Lower concentrations of iodide, similar to those used in the UV-vis experiments, could be probed with micro-electrodes. Careful experimental control could yield valuable quantitative data.

5.0 Modeling

The modeling work aimed to translate the experimental results into trends that relate iodine speciation and volatility to the processing parameters associated with ^{99}Mo production. The kinetic models are discussed above (Section 2.2.1). The process parameters and the values investigated are summarized in Table 6. The full parameter space was explored with the exception that iodine was introduced either as an iodide concentration at the start of the simulation or through a generation term (iodide generation rate) –

only one of the two was nonzero. As a result, 6804 calculations were run. Each simulation covered the span of one week, and the parameters (including the dose rate) were held steady throughout the simulation.

Table 6. Process parameters for kinetic simulations.

Parameter	*Values*
Dose Rate (Mrad/hr)	0.1, 0.5, 1.0
Solution Volume (L)	10, 50, 100
Headspace Volume (L)	5, 25, 50
Interfacial Area (dm^2)	0.1, 0.5, 1.0
Gas Flow Rate (L/s)	0.1, 1.0, 10
$[I^-]_0$ (mol/L)	1×10^{-8}, 1×10^{-7}, 1×10^{-6}, 1×10^{-5}
Iodide Gen. Rate (mol/s)	5×10^{-11}, 1×10^{-10}, 3×10^{-10}

The units for interfacial area (dm^2) are uncommon, but they are necessary for consistency within the model. Multiplying these values by 100 gives the value in cm^2, dividing by 100 gives the value in m^2, and multiplying by 15.5 gives the area in in^2.

5.1 Irradiated Iodide Solutions

Modeling solutions defined by an initial concentration of iodide gives a first analysis of how process parameters can influence the oxidation of iodide into other chemical forms including I_2 vapor. However, the first step of this analysis looks at how much of the initial iodide is oxidized to *any* other species. Figure 21 shows how the fraction of iodide converted to other forms changes with solution volume, gas flow rate, and dose rate. In the simulations presented, the headspace volume was 50 L, the interfacial area was 1.0 dm^2, and the temperature was 5°C.

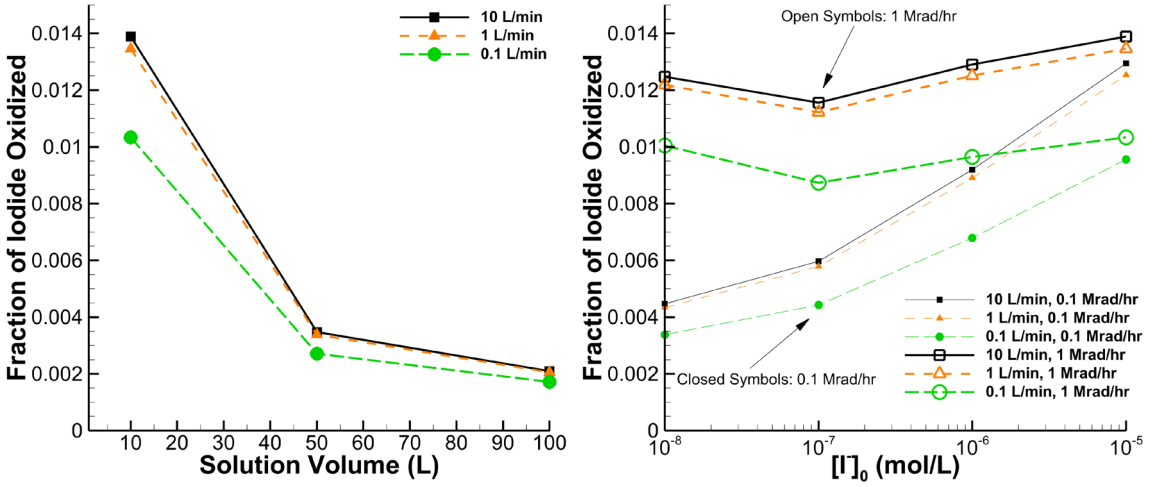

Figure 21. Fraction of iodide oxidized as a function of solution volume at a dose rate of 0.1 Mrad/hr for a $1x10^{-5}$ M NaI in 0.5 M H_2SO_4 (left) and initial iodide concentration (right).

The results show that the iodide is more difficult to oxidize when there is a larger volume of solution despite the concentration remaining the same. Increasing the initial iodide concentration generally increases the amount of iodide oxidized, but the effect is more pronounced at 0.1 Mrad/hr than at 1.0 Mrad/hr. Over the entire set of process parameters investigated, at most 1.4% of the iodide was converted into other

species. Low conversions are consistent with the experiments above that showed negligible absorbance for I_3^- and I_2 when NaI was exposed to H_2SO_4. Though not shown, increasing the interfacial area also increases the fraction of iodide oxidized. This is readily explained by the fact that greater interfacial area increases the mass transfer rate of I_2 into the vapor phase.

Results for the irradiated solutions of NaI in H_2SO_4 media indicate that the dose has minimal effect on pH and makes the solution more oxidizing (though not strongly oxidizing). In the simulations, the pH is changes by approximately 0.01 units. The solution potential, however, changes significantly because of the model's structure. All reactions involving electrons and sulfur- or iodine-containing species are irreversible reductions. The only electron source is due to radiolysis. As a result, the solution potential is approximately 0.95 V (vs. SHE).

The volatility of I_2 in this scenario is bound to be small because so little iodide is oxidized. As seen in Figure 22, the fraction of the initial iodide converted to vapor is in the range of 0.1-1.3%.

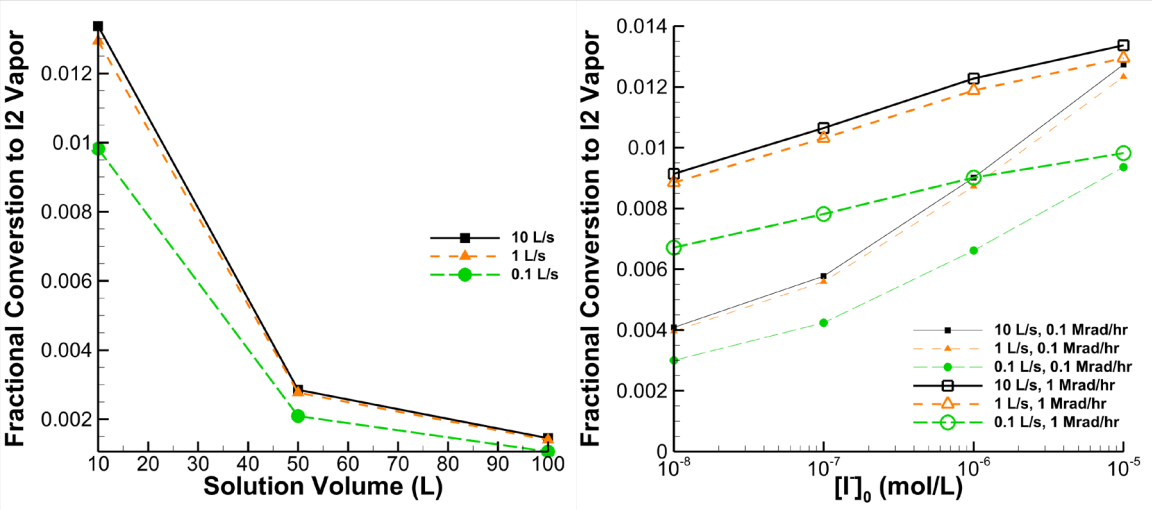

Figure 22. Fraction of total iodine volatilized as a function of solution volume at a dose rate of 0.1 Mrad/hr for $1x10^{-5}$ M NaI in 0.5 M H_2SO_4 (left) and initial iodide concentration (right).

The fraction of iodine that becomes vapor shows the same trend with solution volume as was seen in Figure 21. However, the volatile fraction has a more pronounced trend of increasing with the initial iodide concentration. This is to say that more iodine in the solution leads to a more than proportional increase in the fraction volatilized. Further comparison between the fraction of iodide oxidized in Figure 21 and the fraction volatilized as I_2 in Figure 22 suggests that a large fraction of the oxidized I^- escapes as $I_{2\,(g)}$. Larger solution vessels hinder this, though holding so many other variables constant (instead of scaling with the solution volume) may cause this effect to be overstated.

The final observation from analyzing the various process parameters is to note that the gas flow rate appears to reach a point where I_2 vapor removal is no longer able to drive additional oxidation of iodide or formation I_2 vapor. This is seen in the way the 1.0 L/s and 10 L/s flow rates produce near-identical results. A sufficient, but not excessive, gas flow rate is necessary to sweep the headspace or sparge the solution such that gas containing a negligible amount of I_2.

5.2 Irradiated Solutions with Iodide Generation

In contrast to the previous section, it is also logical to consider the case where iodine in solution is generated through the dissolution of spent fuel or through fission of dissolved uranium. For the purposes of

this analysis, the generation rate may be considered a constant. Furthermore, this analysis assumes that the there is no iodine (of any form) in the solution at the start of the simulation. The generation term assumes that iodide is the chemical form generated. The last assumption may be suspect in the case of iodine derived from the fission of dissolved uranium, but it is reasonable for the case where spent fuel is dissolved.

As before, the purpose of this analysis is to consider how much of the iodide is converted to other forms and the extent to which it leads to I_2 vapor. The results (Figure 23) don't show that there is any significant change from the trends reported in the previous section.

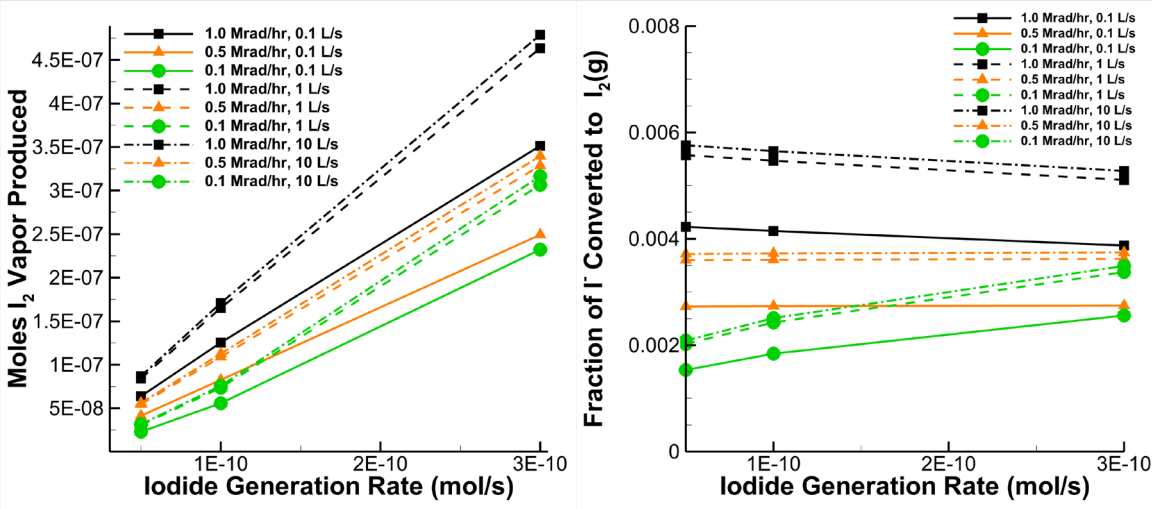

Figure 23. Moles of $I_{2\,(g)}$ generated (left) and the fraction of I^- converted in $I_{2\,(g)}$ (right) as a function of the I_2 generation rate in a 0.5 M H_2SO_4 solution. Dose rates are 1.0 Mrad/hr (black), 0.5 Mrad/hr (orange), and 0.1 Mrad/hr (green). Gas flow rates are 0.1 L/s (solid lines), 1 L/s (dashed lines), and 10 L/s (dash-dot lines).

The main conclusion that can be drawn from Figure 23 is that the fraction of I^- oxidized to other forms in sulfuric acid is minimal (maximum 0.6%). Higher dose rates lead to higher quantities of $I_{2\,(g)}$ formation. Increasing the iodide generation rate results in more moles of $I_{2\,(g)}$ formed because there is a larger amount of iodine in the system. However, there is very little change when the fraction of iodide converted to $I_{2\,(g)}$ is inspected. Higher gas flow rates (dash-dot lines) always lead to higher amounts of $I_{2\,(g)}$ when other process variables are held constant. However, there are diminishing returns as the gas flow rate increases as seen by the way the 1 L/s and 10 L/s flow rates start to give similar amounts generated.

Given the similarity between these results and those in the previous section, the choice of modeling the system using a generation term compared to assuming an initial iodide concentration makes no significant difference when looking at trends. Should the time-dependent concentrations and vapor quantities be desired, the resulting curves will differ because of the way the iodide is added to the system.

5.3 Model Limitations

The model used in the preceding section has some limitations that should be considered when analyzing the results. The kinetic model was derived from a group of sources whose consistency should be further evaluated. Any kinetic model is limited by the elementary steps included and the quality of the rate constants for these reactions. In this case, the LIRIC 3.2 model coupling radiolysis and hydrolysis to the transformation of iodine [Wren and Ball, 2001] was developed for a range of moderate pH values (5-10) and is still being validated for more acidic conditions.

The direct radiolysis of sulfuric acid was not included in the reaction scheme. To do so would require incorporating additional kinetics and partitioning the dose rate between the water and sulfuric acid. Instead, transformation of sulfuric acid was assumed to proceed via radiolysis products from water (mainly, O_2, H_2, and H_2O_2). Concentrations of radiolytic products in pure water computed by Pasting and Laverne (2001) showed general agreement with those from the LIRIC model [Wren and Ball, 2001. In solutions with significant sulfate present, the electron fraction of the sulfate (also bisulfate and sulfuric acid) will result in the formation of radicals that may change the pathways or inhibit/delay the transformation of iodide by consuming radicals generated through radiolysis of water. Furthermore, the as-implemented kinetics of hydrolytic transformation of sulfate-derived species does not contain any temperature dependence. Whether this influences the iodine transformation kinetics is nebulous at this time.

6.0 Conclusions

Managing the release of fission gases continues to be a major concern during the production of ^{99}Mo from uranium targets. Iodine presents a unique challenge, capturing this fission product allows for direct control of a delayed radioxenon source term, while iodine possess multiple isotopes that each pose their own health and safety hazards. The work presented builds upon the work from previous years, working to build a predictive model of iodine behavior in solution.

Iodine speciation is highly complicated, capable of existing as multiple oxidation states, in multiple different molecular forms. Complexities of the systems used to produce ^{99}Mo precluded the use of existing thermodynamic models, instead requiring the development of a kinetics models to address lifetimes of chemical species and a system well outside of equilibrium. To aid in the development, we investigated solutions of NaI and $NaIO_3$ in increasingly complex matrices. These investigations started in water, introducing H_2SO_4, the addition of H_2O_2 as a radiolysis surrogate, and finally culminating in solutions irradiated using the PNNL ^{60}Co gamma irradiator, probing the iodine speciation using spectroscopic techniques.

Our investigations indicated that within the H_2SO_4 system, the iodine speciation is well controlled and largely stable as I^- without an oxidizing agent (e.g. HNO_3) in solution. The introduction of H_2O_2 produced the expected oxidation of I^- to I_2, in quantities that appear to be qualitatively similar to those seen in the irradiated solutions. Though further study is likely necessary, H_2O_2 use as surrogate for radiolysis of water is within reason for this system. This was further supported through a study of the kinetics of iodine speciation changes with the addition of H_2O_2, where it was found over the course of time I^- will be oxidized and the speciation will change from I_3^- to I_2. Iodine oxidation with the inclusion of a radiolysis or radiolysis surrogate, highlights the need for iodine control in a H_2SO_4 matrix even though the oxidation to higher oxidation states in these solutions is lower relative to other matrices such as HNO_3. To further probe the electrochemistry from a mechanistic perspective, we conducted a series of electrochemistry studies that highlights the complicated nature of the iodine with some investigations of the kinetics of the oxidation.

Incorporation of kinetics and radiolysis into our models enabled the models to be predictive of the speciation of iodine, where the thermodynamic models failed. Modeling of iodine speciation under process conditions including an applied dose and vapor-liquid interface indicates that very little iodine vapor should be generated from a H_2SO_4 solution. At most 1-2% of the iodine present will transform into $I_{2\,(g)}$. The main process variables that influence the volatile iodine are the gas flow rate (either sweeping or sparging the vessel). Increasing the solution volume can also reduce the fraction of iodine vaporized assuming all other process parameters remain constant. Consistent with experimental results in sulfuric acid, there is minimal capacity for iodide to be oxidized. Therefore, one should expect the iodine in solution to follow the aqueous stream leaving the vessel. This conclusion only applies to iodide in sulfuric acid.

Our efforts to decipher the complexities of iodine speciation with a dissolved ^{99}Mo fission target have established a robust foundation for a predictive understanding the chemistry of iodine within the extreme environment of a solution under high radiolytic stress. This work has equipped us with the tools and means to better capture and control fission product iodine by predicting its chemistry, assuring the health, safety and regulatory requirements can be met by producers in their pursuit of establishing a stable source of domestic ^{99}Mo.

7.0 References

Bard, A. J., L. R. Faulkner. 2001. Electrochemical Methods: Fundamentals and Applications, 2nd ed. John Wiley & Sons, Inc., Hoboken, NJ p. 97.

Caer, Le. 2011. "Water Radiolysis: Influence of Oxide Surfaces on H2 Production." *Water* 235-253.

Cantrel, L., R. Chaouche, J. Chopin-Dumas. 1997. "Diffusion Coefficients of Molecular Iodine in Aqueous Solutions." *Journal of Chemical Engineering Data*, 42, 216–220.

Criquet, J. and Leitner, N.K.V. Electron beam irradiation of aqueous solution of persulfate ions. *Chemical Engineering Journal.* **169**, 258-262 (2011)

Gartman, B., Branch, S.., Pratt, S., Ritzmann, A., Bautista, A., Rakos, J., Murphy, M., Heine, M., Uhnak, N. 2023. PNNL-35047 Iodine Speciation Under Radiolysis in Nitrate Media. Richland, WA: Pacific Northwest National Laboratory.

Graham, T.R., B.N. Gartman, A. Bautista, L.E. Irwin, E.J. Shelby, D.L. Saunders, T.J. Johnson, et al. 2023. "Spectroscopic features of dissolved iodine in pristine and gamma-irradiated nitric acid solutions." *Journal of Molecular Liquids* 122631.

Iwamatsu, K., Sundin, S., LaVerne, J., "Hydrogen peroxide kinetics in water radiolysis". *Radiation Physics and Chemistry.* 145, (2018) 207-212

Jiang, P.-Y., Katsumura, Y., Nagaishi, R., Domae, M., Ishikawa K., and Yoshida, Y. "Pulse Radiolysis Study of Concentrated Sulfuric Acids." J. Chem. Soc., Faraday Trans., 1992, 88, 1653–1658

Koppenol, W.H., D.M. Stanbury, and P.L Bounds. 2010. "Electrode potentials of partially reduced oxygen species, from dioxygen to water." *Free Radical Biology & Medicine* 317-322.

Ma, J. Schmidhammer, U. Mostafavi, M. Picosecond puls radiolysis of highly concentrated sulfuric acid solutions: Evidence for the oxidation reactivity of radical cation $\bullet H_2O^+$. *Journal of Physical Chemistry A*. **118**, 4030-4037. (2014)

Nicholson, R. S. 1965. "Theory and Application of Cyclic Voltammetry for Measurement of Electrode Reaction Kinetics." Analytical Chemistry, 37(11), 1351–1355.

Pastina, B., and J.A LaVerne. 2001. "Effect of Molecular Hydrogen on Hydrogen Peroxide in Water Radiolysis." *Journal of Physical Chemistry A* 9085-9322.

Sawai, T., Shinozaki, Y., Meshitsuka, G. "The Radiolysis of Aqueous Solutions of Potassium Iodide". *Bull. Chem. Soc. Jpn*. **39** (1966). 951-955.

Tenchurina, A.R., Sal'keeva, A.K. Radiolysis and photolysis of sodium sulfate crystalline hydrate. *Russ. J. Phys. Chem.* **90**, 688–690 (2016).

Virtanen, P., et al. SciPu 1.0: Fundamental Algorthms for Scientific Computing in Python. *Nature Methods* **17**, 261-272 (2020)

Wang, J. 2000. *Analytical Electrochemistry, 2nd ed.* Wiley-VCH, New York.

Wren, J.C., Ball, J.M. LIRIC 3.2 an updated model for iodine behaviour in the presence of organic impurities. *Radiation Physics and Chemistry*, **60**, 577-596 (2001)

Wojnárovits, L. and Takács, E. "Rate constants of sulfate radical anion reactions with organic molecules: A review. *Chemosphere*, **220**, 1014-1032 (2019)

Yaraliev, Ya. A. "Electrochemistry of Iodine" *Russian Chemical Reviews*, 51(6), 566–580.

Appendix A – Title

A.1 Calculation of H_2O_2 as radiolysis surrogate

$$709kGy\ x\ \frac{1000Gy}{1kGy} x\ \frac{1Jkg^{-1}}{1Gy}\ x \frac{1kg}{1000g} x \frac{1g}{1mL}\ x \frac{1000mL}{L}\ x \frac{0.28\mu mol\ \square OH}{J}\ x \frac{1mol}{1x10^6\mu mol}\ x\ \frac{1molH_2O_2}{2mol\square OH} = 0.01\ M\ H_2O_2$$

Pacific Northwest National Laboratory

902 Battelle Boulevard
P.O. Box 999
Richland, WA 99354

1-888-375-PNNL (7665)

www.pnnl.gov